Conceptual and Preliminary Design of a Long Endurance Electric UAV

Luís Miguel Almodôvar Parada
luisparada2@hotmail.com

Instituto Superior Técnico, Universidade de Lisboa, Portugal

November 2016

Abstract

The present thesis documents the conceptual and preliminary design of a solar long endurance Unmanned Aerial Vehicle (UAV). Having in mind surveillance goals, the mission profile requires an initial climb, at a rate that allows to ascend 1000 m above runway in 10 minutes, followed by cruise with an endurance of 8 hours and a range 200 km during the equinox. In the conceptual stage, several aircraft configurations were evaluated considering the mission requirements. Resorting to the Analytic Hierarchy Process methodology, the rear pusher V-tail airplane concept was chosen through pairwise comparisons between 10 mission criteria (Aerodynamics, Structures an Weight, Solar Panels Integration, Propulsion, Manufacturing and Maintenance, Stability and Control, Payload Volume, Remote-Person View Integration, Take-off and Landing and Portable Capabilities) and 8 prospective candidate configurations. A UAV market investigation provided an initial estimate of the empty weight fraction and airframe dimensions. Through bibliographic research, the communications system was defined beforehand and the propulsion system also received an initial estimate. In the preliminary design phase, the airframe was resized by performing a set of fixed point iterations, whose resulting design point ensured it is physically possible to fulfill flight requirements. Allying multiple aerodynamic analyses, performed on a low Reynolds number computational tool, with the ascertained efficiency of the propulsion system, power consumption at each mission stage was determined under ideal weather conditions. The solar energy received by the photo-voltaic arrays installed was determined in a single location applying a theoretical irradiation model in different seasons of the year. It was verified that in the March equinox endurance reached 7.5 hours, while in September its maximum increased to almost 10 hours. An aircraft CAD assembly was modeled without internal airframe detail. The developed parts include a three-piece 5 meter span wing, a fuselage composed by two connectable pieces, totaling 1.9 meter length, and two individual V-tail halves. On-board propulsion and avionics components were also modeled in a simplified way, as solids of uniform density. A flight stability analysis was performed, resulting in a static margin of 5.6% with null C_m in cruise conditions. Looking at a future detailed design, the cruise flight envelope was created and the wing pressure distribution was obtained.

Keywords: Solar UAV, Analytic Hierarchy Process, Design Point, Low Reynolds Number, Endurance, Flight Envelope.

1. Introduction

Usage progress of UAVs for civil applications is not steadily established because, unlike in the defense sector, where air space is properly prepared and the completion of the mission is supra to the economics of the vehicle, for civilian procedures cost sustainability and operational complexity are still major barriers. Most existing mission profiles for modern UAVs require a platform, or series of platforms, which clearly extend range and endurance beyond the capability of existing affordable electric vehicles.

At the same time, the use of renewable energies in vehicles is becoming more and more demanding by society due to its growing environmental awareness. Taking this factors into account, it has become clear in the last years that the key to enhance UAVs long endurance capabilities can be found within solar aviation. Nowadays, with the relatively easy access to numerical and experimental design tools and with the current efficiency of electric systems (solar panels, motors and batteries) there is a real chance to expand UAVs applications. The aim of this thesis is to achieve the preliminary design of a solar powered UAV, meant to be used for civilian surveillance missions.

2. Project Background

This work started as a part of a project of a Long Endurance Electric Unmanned Aircraft Vehicle (LEEUAV) that is being developed with the collaboration of IDMEC (Instituto de Engenharia Mecânica), INEGI (Instituto de Ciência e Inovação em Engenharia Mecânica e Engenharia Industrial) and AeroG (Aeronautics and Astronautics Research Center). All units involved are a part of Laboratório Associado de Energia, Transportes e Aeronáutica (LAETA). The main goal of the project is to develop a low cost, small footprint electric UAV, easy to build and maintain, that can be deployed from short airfields to perform long endurance surveillance missions [5]. To remain airborne for extended periods of time the aircraft must harbor green power technologies, such as an electric propulsion system with solar power.

2.1. Accomplished Tasks

To assist the complete design of the LEEUAV, there are several tasks from different areas that have been addressed beforehand.

Two master students, Héctor Vidales and Tiago Ferreira, have poured over the propulsion system design for the LEEUAV, as part of their published dissertations [9, 3]. Different electric configurations have been evaluated in terms of performance, overall weight and cost. The selection of solar panels was followed by the specification of possible brushless motors. A hybrid propulsion system ended up being established due to the necessity of a secondary energy source, in the form of high-density rechargeable batteries, to power climb flight.

A first generation prototype has been built under a master's thesis from UBI written by Luís Cândido [2], using advanced model building techniques. Construction tests allowed to reach relevant conclusions related to applicable materials and manufacturing processes. Flight tests were also performed in radio controlled mode. In spite of not harboring the solar energy collection system and all avionics components, the aircraft allowed to obtain important qualitative performance knowledge for a prospective solar UAV configuration.

Regarding aerodynamics, a computational process enabling high fidelity fluid analysis of different UAV configurations has been developed by Nuno Silva, as part of his published master's dissertation [8]. As a case study, the aerodynamic behavior of the first generation built prototype, a conventional configuration, was evaluated for cruise conditions.

In the field of communications and electronics, the Autopilot and Remote Person View (RPV) hardware and software design have been addressed in two published master thesis, written by Duarte Figueiredo and Pedro Miller, respectively [4, 6].

3. LEEUAV Concept

In the Conceptual Design different configurations are evaluated to meet or exceed the mission requirements in terms of endurance, size and cost.

3.1. Project Requirements

The particular requirements of the LEEUAV project were deliberated assuming that atmospheric parameters vary according to the International Standard Atmosphere model. The mission starts with take-off followed by climb until a maximum steady flight altitude of 2000 m. Climb occurs at a minimum rate of 1.667 m/s during 10 minutes, which allows to ascend 1000 m. Bearing in mind that flying at 2000 m over most Portuguese locations would not allow the RPV camera to record ground footage with acceptable resolution display, the project service ceiling was fixed at 1300 m.

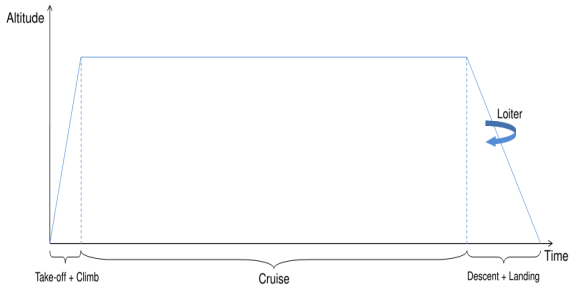

Figure 1: Scheme of the LEEUAV mission.

Cruise is the longest phase of the mission, represented in Figure 1, in which there must be a time window of 8 hours during the equinox to fly over specified locations and to turn around, reaching a range of 200 km after returning to base. Considering both range and time constraints, the project's cruise speed selected is 7.53 m/s. Occasionally, loiter may be needed before landing. The minimum bank angle for the aircraft's turn is 45°, with an associated load factor of 1.414.

The LEEUAV must also be able to carry a payload of up to 10 N, this includes all components of the communications systems and extra equipment, such as measurement sensors. The aircraft's dimensions must allow operations in very small airfields (eventually no airfield will be required) and it has to possess portable capabilities suitable for small vehicle ground transportation.

3.2. Conceptual Design Selection

A total of 8 prospective aircraft configurations, illustrated in Figure 2, have been selected attending to the mission profile and project background.

The airframe alternatives were chosen with the purpose of evaluating conjugated effects of features that did not present clear reasons to be excluded beforehand. The quadcopter is an exception that was

chosen to demonstrate how the Analytic Hierarchy Process precludes an evident poor solution.

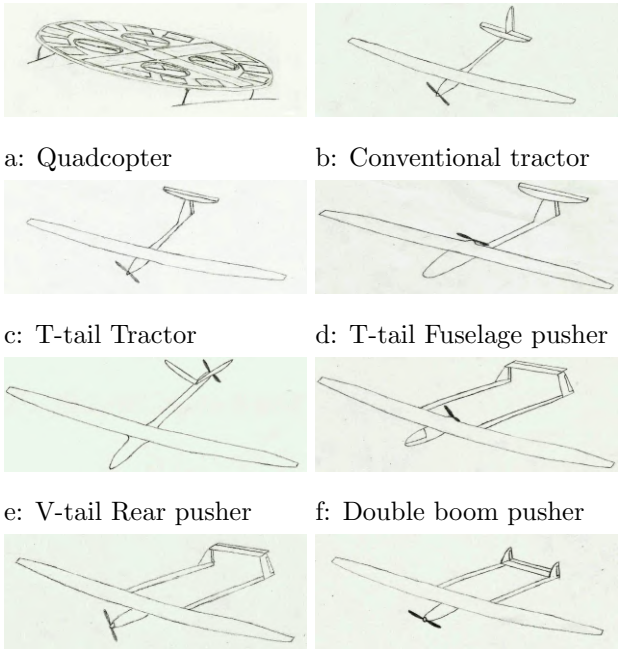

a: Quadcopter b: Conventional tractor

c: T-tail Tractor d: T-tail Fuselage pusher

e: V-tail Rear pusher f: Double boom pusher

g: High tail double boom tractor h: Low tail double boom tractor

Figure 2: Selected airframe alternatives.

3.3. Analytic Hierarchy Process Based Decision

The selection of the aircraft configuration was carried out using an Analytic Hierarchy Process (AHP) [7]. With this decision making methodology, a set of criteria and alternatives underwent several pairwise comparisons in order to select the most suitable UAV configuration for the mission requirements.

On the AHP method pairwise comparisons are made using a scale that consists of qualitative judgments ranging from equal to extreme with corresponding numerical values (1 = equal , 3 = moderate, 5 = strong, 7 = very strong, 9 = extreme importance). A pairwise comparison matrix A was initially filled with the numerical judgments for criteria, respecting the reciprocal property ($a_{ij} = 1/a_{ji}$). The priorities of the elements were estimated by finding the principal eigenvector of matrix A, $AQ = \gamma_{max}Q$, where γ_{max} is the maximum eigenvalue of matrix A. When vector Q is normalized, it becomes the priority vector. While building a pairwise comparison matrix, it is necessary to check consistency by calculating consistency ratio (CR) as the ratio of Consistency Index (CI) with Random Index (RI), a tabulated value. Consistency Index is calculated by $CI = (\gamma_{max} - d)/(d-1)$, where d is the square matrix dimension. Inconsistencies are tolerable and a reliable result may be expected if $CR < 0.1$.

The global priority pie chart division (Figure 3) reveals three major criteria, Aerodynamics, Structures and Weight and Solar Panels Integration, which affect range the most.

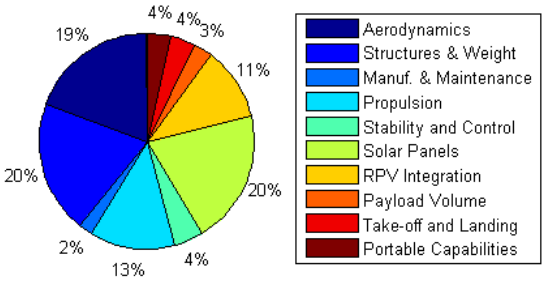

Figure 3: Global Priority Vector Results.

The same eigenvalue computing process was used to determine the comparison matrices of the candidate configurations with respect to the criteria and their local priorities. All ten pairwise comparison matrices of alternatives, as well as the global priority data matrix with respect to criteria, have been placed in the main document of this work. The consistency ratio always remained acceptable ($CR < 0.1$).

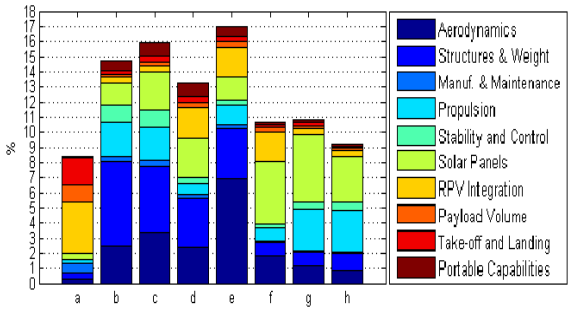

Figure 4: AHP Final results (the bar numbering matches the configurations in figure 2).

The final priority vector was obtained by multiplying the matrix of local priorities with the global priority vector , providing the raking of alternatives, illustrated in Figure 4. After adding up all scores, the overall winner of the AHP was the rear pusher with V-tail (Figure 2e) that got a preference of 17%, surpassing the second classified, the T-tail tractor, by a margin of 1%. The decisive factor was aerodynamics, that was the only criteria where the rear pusher excelled over the remaining alternatives.

4. Aircraft Initial Sizing

With the concept decided, a first estimation of the LEEUAV's dimensions and weight was carried out.

4.0.1 Empty Weight Estimation

A market research was conducted to find empty weight fractions of low wingspan UAVs with dimen-

sions similar to the first generation prototype. The research focused mainly on model gliders (with electric propulsion or not), due to their high aspect ratio and absence of landing gear.

Within the arranged database, three major wing construction types were identified: Foam Cored Construction, Molded Construction and Rib Construction.

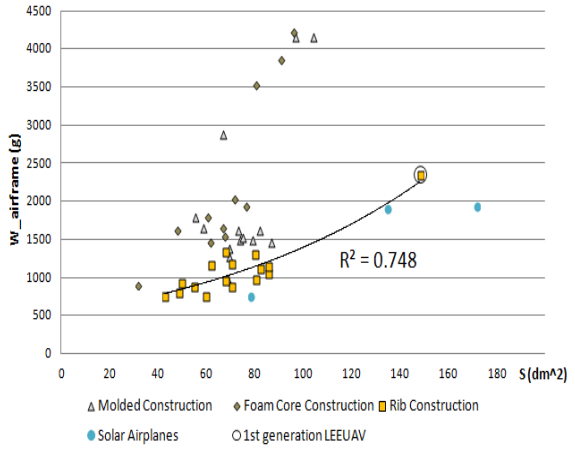

Figure 5: Empty weight as function of wing area obtained with model glider scattered data.

The scatter chart in Figure 5 displays the appointed empty weight and wing area of the researched aircraft. It is noticeable that models with rib conceived wings tend to be lighter for the same wing area. For that reason, the rib construction type should be selected for the wings manufacture, as it had been previously for the first generation LEEUAV.

In spite of the observable gap between values, it was possible to interpolate an expression relating empty weight with wing area, while keeping a fair correlation coefficient.

$$m_{airframe} = 512.99\ e^{0.01\,S} \tag{1}$$

Intelligibly, Equation (1) was obtained using solely points that correspond to rib constructed wings.

The few solar planes found also have rib constructed wings, but none was used as an interpolation point because their weight values were considered too optimistic. The lack of further examples with wing dimensions superior to that of the first LEEUAV reduces the calculation accuracy, since the airframe weight is expected to fall outside the range of interpolation.

4.1. LEEUAV Provisory General Characteristics

The first generation LEEUAV was a guideline to assign general dimensions beforehand. It allowed to determine that there would be wing tip portion without solar arrays, solely meant for aileron control, while on the remaining wing surface, solar arrays would fill as much area as possible. The V-tail was initially sized as an equivalent conversion from the first generation's conventional tail. Its planform area and dihedral angle were calculated under the assumption that V-tail's aspect ratio equals that of its conventional counterpart's horizontal tail.

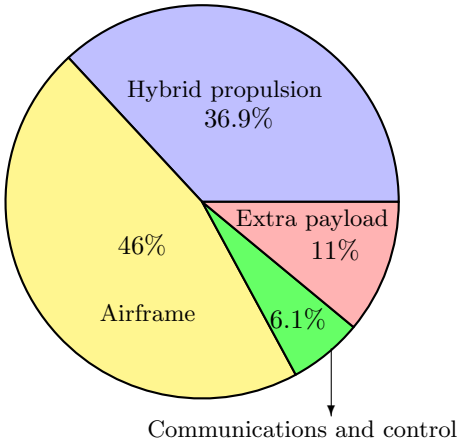

Figure 6: LEEUAV's relative mass distribution.

Altogether, with the mass of all on-board components and airframe, an estimate of the complete weight distribution was obtained in advance. The weight proportions present in Figure 6 are converged values that resulted from the completion of the preliminary project. The airframe percentage includes not only the wing and V-tail but also the fuselage. The hybrid proportion system covers all components directly relate with thrust generation (propeller, motor, electronic speed controller), energy storage (batteries) and energy collection (solar panels and Maximum Power Point Tracker). As for the smaller slice, the communications systems, it comprises the video system, the autopilot and all electronic components associated. It should be noted that the sum of the extra payload weight with communication components yields a value close to the maximum payload of 10 N specified on the mission requirements.

5. Preliminary Project

The preliminary project aims to define the overall dimensions of the aircraft, as well as the propulsion system and general placement of all components.

5.1. Aerodynamics

To enable a swift processing of aerodynamic results, an open source software called XFLR5 was chosen. Its capabilities include 2D airfoil direct analysis as well as 3D wing analysis based on several methods at choice including the Lifting Line Theory (LLT), the 3D Panel Method and the Vortex

Lattice Method (VLM).

5.1.1 Aerodynamic Software Accuracy

Unlike Panel Method and LLT, VLM is capable of producing results for wing and tail geometries with low aspect ratio and high dihedral. Therefore, it was the chosen 3D analysis method. To verify the accuracy of VLM, XFLR5 was employed with airflow characteristics and lifting geometries similar to the ones used in the high fidelity CFD analysis made for the first generation LEEUAV in steady flight[8]. The results of both software were compared afterwards.

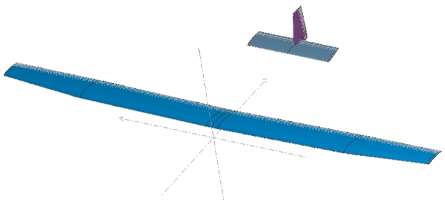

Figure 7: Geometry considered in XFLR5.

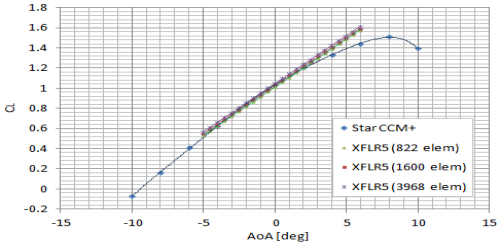

(a) C_L as function of α.

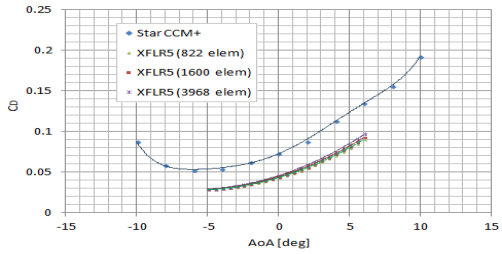

(b) C_D as function of α.

Figure 8: Original LEEUAV cruise performance charts (U=7.53 m/s) [8].

In all simulations computed on XFLR5, both wing and tail are the only aerodynamic geometries present (figure 7). Incorporating a fuselage is not recommended by software developers, as the results of its aerodynamic influence are generally not very satisfactory. Still, XFLR5 results are known for being reasonably accurate for model sailplanes operating at low Reynolds Numbers.

This software allows the user to control the density of the computational grid, always with rectangular divisions, within a certain range of panel elements. Three grids were generated for this study, having 822, 1600 and 3968 elements.

Figure 8a shows that the lift predicted in XFLR5 is rather accurate, when compared with STAR-CCM+®, for angles of attack between -5° and 2°. On the other hand, figure 8b confirms that XFLR5 underpredicts global drag coefficient real values. This outcome was expected since XFLR5 utilizes information within previously XFoil-generated polars, at several Reynolds number, to extrapolate the 3D viscous drag component. For this same reason, the airplane performance outputs do not include results close to stall angles. In this analysis the computed angle of attack has been limited to values between -5° to 5.5°. A closer inspection on the output files revealed that shear and pressure components of drag were underpredicted by VLM.

Overall, it was observed that a grid with 1600 elements provides the best compromise between accuracy and computation time. Therefore, for those specific analysis results, in Figure 8, correction functions were calculated, assuming the form $Z_x(\alpha) = C_x(\alpha)_{STAR-CCM+}/C_x(\alpha)_{XFLR5}$, where x is either lift (L) or drag (D). To recoup for XFLR5 output discrepancies, Z_x functions were applied to all XFLR5 3D analysis performed. The practical purpose of this correction is achieved by improving the XFLR5 output margin of error while rearranging lift and drag predictions, for angles of attack between -5° and 5.5°, more conservatively.

5.2. Cruise Stage Computation

The aerodynamic geometries (wing and tail) of the LEEUAV conjectured on the initial sizing went trough VLM computational analysis in order to assure that in steady flight the maximum take-off weight (MTOW) breaks even with the lift produced.

At the beginning, the geometry update focused solely on the wing. As adjustments were being made and reinserted in XFLR5, the airframe weight was recalculated with Equation (1) and the wire length linking servos updated as well. The whole process, illustrated by the flowchart in figure 9, was reiterated until MTOW equaled the lift computed aerodynamically.

Chordwise there were not any changes on the wing, because increasing the mean chord would admittedly enlarge the existing gap between MTOW and produced lift at cruise speed. Conversely, raising the wingspan beyond the mark of five meters could narrow down that difference, however, that possibility was not embraced since it would add further structural and transportation issues.

Instead, the approach followed was to modify the wing's airfoil. Formerly it had a curvature of 5.3%, which was renewed to 7.5% so that its lift coefficient raised. Envisioning difficulties related to the

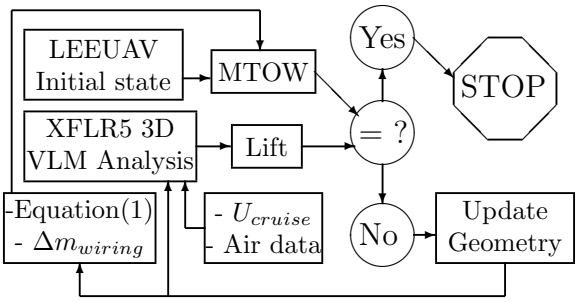

Figure 9: Initial Aerodynamic iterative scheme for cruise stage.

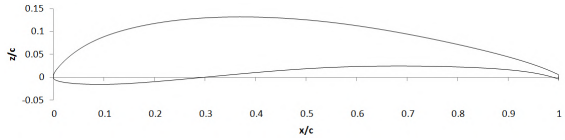

Figure 10: Updated wing airfoil of the LEEUAV, $t/c = 13\%$.

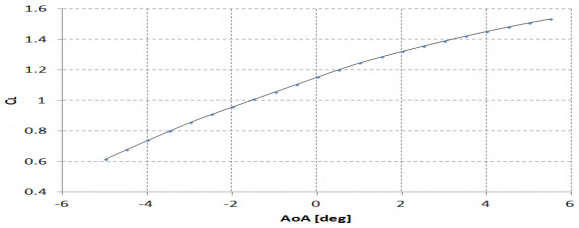

(a) C_L as function of AoA.

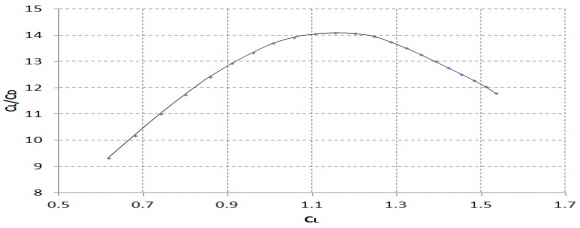

(b) C_L/C_D as function of C_L.

Figure 11: LEEUAV aerodynamic performance charts (U=7.53 m/s).

prototype's construction, the airfoil relative thickness was increased to 13%, as seen in figure 10.

Initially, the wing had an constant incident angle of attack of 5º, which was modified with washout. It has been proved, in [8], that, at higher angles of attack, this feature may reduce flow separation in the wing region where the ailerons are located. The torsion applied diminished the angle of attack in 4º, starting on the aileron sections, which resulted in a wing angle of attack of 1º on the tip and 5º on the sections with constant chord.

The definitive lift and drag data, computed at cruise velocity, is shown in figure 11 for all simulated angles of attack. A total of twenty two angles of attack were simulated from -5º to 5.5º, with increments of 0.5º on XFLR5, using VLM method.

In steady flight ($\alpha_{airplane} = 0º$, $\alpha_{wing} = 5º$), the lift coefficient is rounded to 1.153 . Due to computational limitations mentioned in Section 5.1.1 it was not possible to determine both maximum lift and minimum drag coefficients, so those values were estimated, on a conservative way, whenever necessary. To maximize the airplane's range, the aircraft must fly at at angles of attack close to 0º.

5.3. Stability and Control

To support airworthiness towards long endurance missions at low speed, natural longitudinal stability was targeted by fulfilling two design prerequisites. Assuming a longitudinal axis with origin upstream and pointing towards the tail, the center of gravity (CG) was placed behind of the neutral point (NP). Which means the static margin K_n was assured positive, that is

$$K_n = \frac{x_{NP} - x_{CG}}{MAC} > 0 \quad (2)$$

, where x_{NP} and x_{CG} are the longitudinal positions of the neutral point and center of gravity, respectively, and MAC is the mean aerodynamic chord.

At the same time, the V-tail was arranged to counteract the moment that comes from the wing, so that the overall moment coefficient is kept close to null in steady flight conditions.

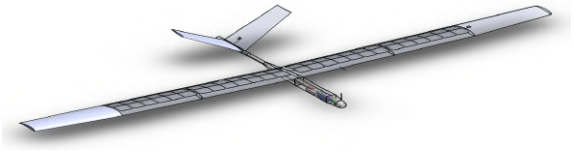

Figure 12: LEEUAV assembly drawn in CAD software SolidWorks®

Resorting to CAD software SolidWorks, the second generation LEEUAV and the majority of onboard components were modeled, as shown in figure 12, and the respective mass centers positioning pinpointed from there. Then, the airplane's updated inertia was transferred to XFLR5, where components and parts, excluding wing and tail-plane, were replaced by punctual masses.

The VLM analysis loop was resumed with incremental modifications in the weight distribution and V-tail characteristics until the results indicated that the longitudinal stability prerequisites were accomplished. Figure 13 illustrates the whole procedure, which also includes the previous aerodynamic loop for cruise (figure 9) to attest that lift keeps matching with flying weight.

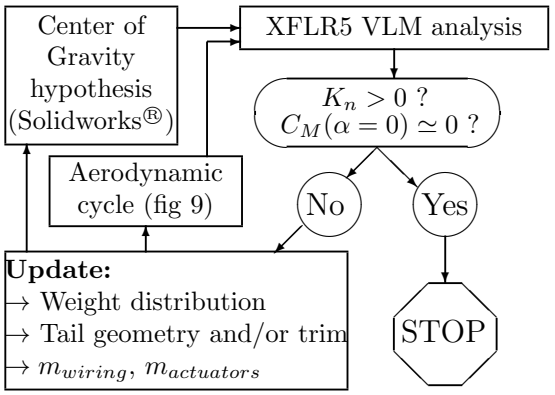

Figure 13: Static stability iterative scheme.

In order to nullify the moment coefficient at cruise AoA of 0º, the V-tail, featuring a modified NACA0008 with 1mm trailing edge thickness, was trimmed with an incidence negative angle of 3º with respect to the fuselage.

The static margin was calculated with the following equation

$$C_{M_\alpha} = -K_n C_{L\alpha} <=> K_n = \frac{C_{M_\alpha}}{C_{L\alpha}}. \qquad (3)$$

Where C_{L_α} and C_{M_α} correspond to the derivatives of the lift (C_L) and moment (C_M) coefficients with respect to the angle of attack.

In steady flight it is observed that $K_n = 5.6\%$, corresponding to, according to a referential with origin in the leading edge, a CG position at 38.86% of the MAC, which was considered acceptable.

Incidentally, a flaw that is highlighted from this stability study approach has to do with the absence of fuselage weight modifications following dimension updates.

5.4. Propulsion

Short-term climbing flight was the first to be examined. Attending to its short duration with respect to the whole mission, it is always assumed that the solar energy received during that stage is negligible.

At this point, while climb drag is determined with a computational VLM simulation at the respective velocity U_{climb}, thrust is computed as as $T_{climb} = Wsin(\varphi) + D$, where φ is the climb angle and W is the aircraft weight.

The raw power required in every part of the mission was determined knowing the efficiency of the propulsive system components. The propeller's was studied with more detail since it is the only component whose performance is directly affected by aerodynamics. Computed performance data, supplied by a manufacturer, provided estimates of thrust, torque and propeller efficiency over a broad range of model speeds and motor revolutions per minute(RPM). All values of any parameter contained within a certain propeller data file can be represented with a single three dimensional graphic as function of two other listed parameters.

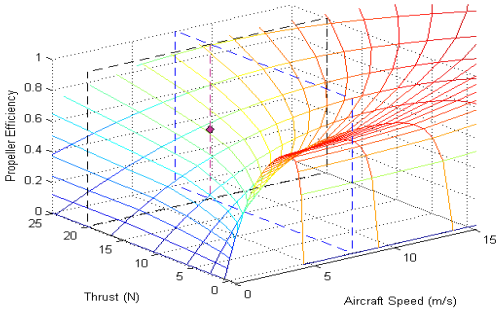

Figure 14: Efficiency graphical calculation of the 15" x 8" propeller with climb regime data.

The propeller efficiency computation is illustrated in Figure 14, where the manufacturer data is the curved surface and the climb regime input is defined by a plane of constant thrust together with a perpendicular plane that assumes constant aircraft velocity. The resulting intersection from those three surfaces yields a point in space that corresponds to the propeller efficiency for the respective flight regime.

	η_{ESC}	η_{Motor}	$\eta_{Propeller}$	η_{prop}
Climb	95 %	89 %	44.8 %	37.9 %
Cruise	95 %	89 %	66.1 %	55.9 %

Table 1: Propulsion sub-system overall efficiency.

Although this study was not extensive, it allowed to select the 15" x 8" composite propeller model, whose efficiency surpasses, in both climb and cruise, all other propellers considered so far. Based on previous propulsion studies [9], a moderate efficiency value of 89% is attributed to the motor. Data regarding the propulsion subsystem efficiency is presented in Table 1, where the ESC, battery and cables receive typical ratings and η_{prop} is the total network efficiency.

The flowchart in Figure 16 sums up how propulsion and energy studies referring to climb are integrated in the design iterative process. In the event of any flight predicament the motor must be able to provide considerably more than enough power to climb, that is $P_{motor} >> P_{prop}$. It was imposed that the battery maximum storage ($E_{battery}$) exceeds the energy needed for the stipulated climb (E_{climb}) in at least 20%. Having this constraint in mind, it was verified that two 3S LiPo batteries, with 4200 mAh each, connected in parallel contain enough energy for a 10 minute climb.

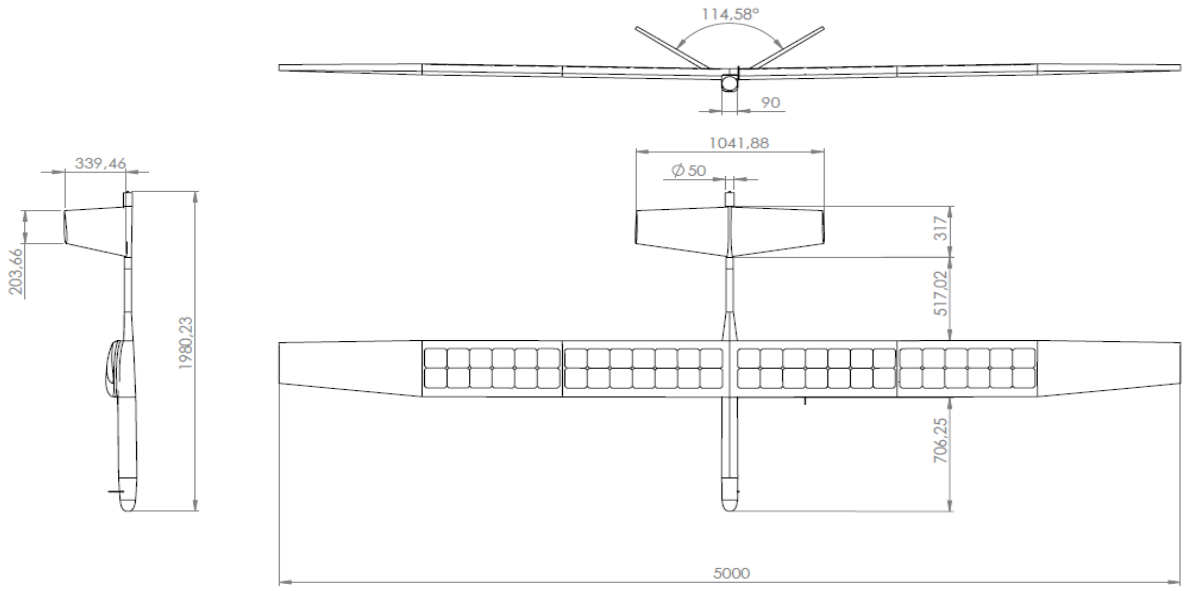

Figure 15: Three view drawing of the LEEUAV, dimensions in mm.

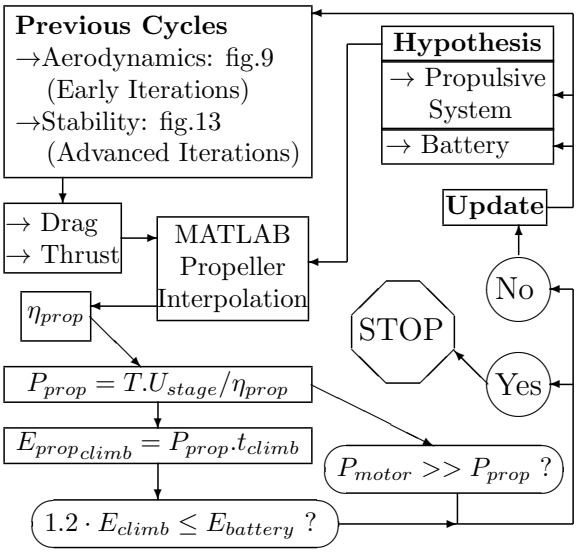

Figure 16: Propulsion and climb energy iterative flowchart.

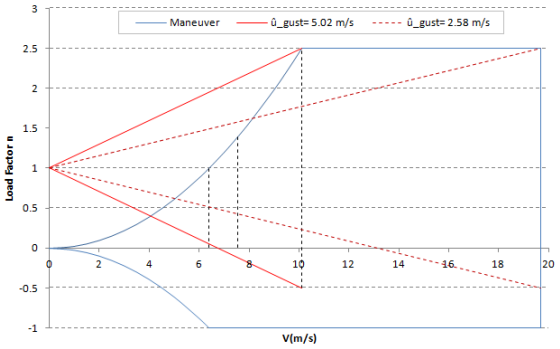

Figure 17: Combined V-n diagram of the LEEUAV, h=1300 m.

5.5. Flight Envelope

The operational framework in relation to air speed and load factor, consisting on the maneuvering and gust envelopes combined in Figure 17, defines the limits for a balanced detailed design of internal structures. The current choice for the load factor upper and lower bounds has been supported by Federal Aviation Regulations (FAR) Part 23 and an available flight envelope of small UAVs with a resembling size, weight and maneuverability [1].

Two main additional scenarios are presented, at the dive speed the aircraft structure cannot withstand gusts that surpass 2.58 m/s, nevertheless, if velocity does not surpass the maneuvering speed the admissible gust raises to 5.02 m/s.

5.6. Design Point

In this work, the design point is intended to indicate the working condition at which the motor can be adapted to its use in the UAV to match the endurance requirement. Therefore, cruise was chosen as the representative situation of the design point.

Observing Table 2, it is clear that the representative design point does not allow the LEEUAV to fulfill climb requirements, thereupon the climb performance specifications have been defined as an off-design switch point. The final overall dimensions of the converged aircraft are presented in Figure 15. Upstream the wing, the fuselage was resized to harbor all components, including the RPV camera upfront. The ailerons and ruddervators were not

drawn since their conceiving involves assembly solutions not addressed at this stage of the project.

W/S	35.26 N/m^2
$(T/W)_{climb}$	0.34
$(P/W)_{climb}$	6.96 W/N
$(T/W)_{cruise}$	0.07
$(P/W)_{cruise}$	1.04 W/N

Table 2: Performance specifications.

6. Solar Energy Management

The design point is highly influenced by the solar energy collection sub-system response to the endurance requirement, that was over-leaped in the iterative process. The efficiency of the photo-voltaic cells (η_{panels}) and Maximum Power Point Tracker (η_{MPPT}), shown in table 3, was estimated based on manufacturer data and experimental tests carried in [3].

η_{panels}	η_{camber}	η_{MPPT}	η_{energy}
20 %	90 %	92%	16.7 %

Table 3: Energy collection sub-system efficiency.

Additionally, an efficiency factor of 90%, η_{camber}, related to the panels camber, was added to cope with the effect the cells with smaller elevation angle have on the whole group of arrays.

A daily irradiation model, explained in more detail in the main thesis document, was arranged for each day of the year in any specified location. The constant set of geographical coordinates chosen correspond to Pampilhosa da Serra, that also served as reference to decide the cruise altitude of 1300 m.

By applying the overall efficiency of the solar energy collection system, η_{energy}, to the irradiance profile, the solar power, P_{solar}, harnessed through solar panels area, A_{solar}, was obtained. Thereafter, knowing the battery energy at the beginning of cruise, $E_{battery}$, and the power consumption, P_{cruise}, flight endurance, Δt_{cruise}, could be computed. The flowchart in Figure 18 illustrates how solar energy calculations have been integrated on the iterative design process.

Both spring and autumnal equinox dates were inserted in the loop and since it is not specified for which one the endurance requirement must be fulfilled, the design is considered converged if cruise surpasses the 8 hour mark in at least one of them. In the advent of not being able to accomplish the endurance requirement, the airplane design would have to be completely reiterated in order to increase the wing area available for solar panels. Fortuitously, the solar energy management loop satisfied the endurance imposition at the first attempt.

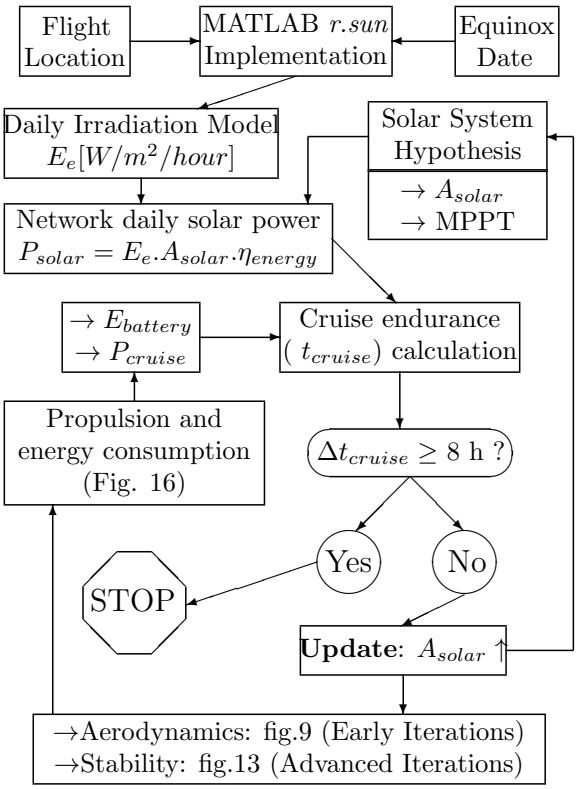

Figure 18: Cruise energy management iterative flowchart.

Figure 19 presents the daily solar net power available in both equinoxes plotted in MATLAB against the power required to cruise. The number of 3S LiPo batteries considered in data treatment ranges from two, that is the standard airborne amount, to three, assuming that the weight of the aircraft does not change.

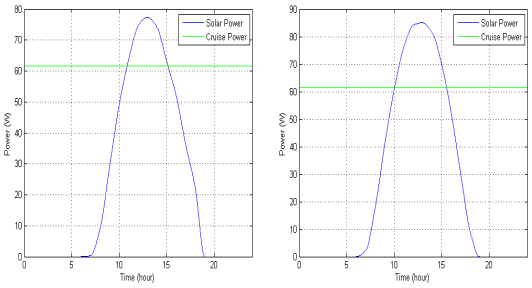

(a) March equinox. (b) September equinox

Figure 19: Power required for steady cruise flight and daily solar net power available during equinoxes in Pampilhosa da Serra (h=1300 m)

On the March equinox, it was established that cruise would start at the hour of the day in which solar power equals the minimum required for steady flight, such instant corresponds to the first intersection between line plots in Figure 19a. In the

long run, all exceeding solar energy can be stored with 2 3S LiPo batteries and used afterwards during the period of solar energy shortage, which leads to an endurance of 7 hours and 34 minutes. The LEEUAV only reaches the 8 hour mark with a third battery in line that is not used for solar energy storage but allows to extend endurance throughout the period of solar energy deficit.

During the September equinox, there is an higher amount of solar power when compared with the March equinox, explained by an increase on the angle of incidence of solar beam irradiation. Although the registered surplus can be contained within 2 empty 3S LiPo batteries, the energy remaining in the storage system after climb would reduce the storage volume available. To prevent extra energy losses, the cruise starting hour was delayed so that when solar power alone allows steady flight the whole storage system is virtually empty. Hence, cruise is initially powered by batteries along with increasing solar power, which maximizes energy storage afterwards. With this, steady flight is prolonged to 9 hours and 58 minutes.

7. Conclusions

In this work the project of a long endurance solar airplane has been carried out, from the conceptual design to the preliminary sizing. Although structural design did not fall under the scope of this thesis, the pressure coefficient wing distribution obtained at this point in XFLR5 can be transferred to a future Finite Element Method (FEM) analysis performed in prospective wing structure proposals. The purpose of the structural project on the overall iterative design procedure is to replace the airframe estimation model, that was given in the initial sizing by Equation (1). Supposing that the detailed design imposes an airframe weight that surpasses the estimate, there is still an error margin assured by the extra payload, visible in Figure 6. Thus, the design point of the LEEUAV is not expected to suffer reiterations due to the detailed design.

As soon as the structural project complete, advanced construction methodologies will have to be found and applied. Experimental techniques can also be arranged to verify the accuracy of FEM computational analysis and to study the residual resistance of the prototype in the presence of defects. At the same time, the take-off system must be engineered. With the prototype built, a set of planned flight tests can be progressively carried on.

Moreover, wind tunnel testing may be used to determine experimentally propulsion efficiency rates that so far have only been estimated, namely the motor's. Regarding aerodynamics, it is possible to virtually eliminate the uncertainty associated to the results obtained in XFLR5 if a CFD computational analysis is performed on the updated airframe geometry. As long as the drag correction applied do not underestimate real values roughly, the current design will still be able to fulfill the mission requirements. Climb performance is expected to end up more changed than cruise's because it depends not only on drag polar computations but also on the estimate made for stall at higher angles of attack.

References

[1] Z. Bessoni and M. Júnior. Structural design of mini-uavs with conventional and alternative materials. In *14th Brazilian Congress of Thermal Sciences and Engineering*. University of Brasilia, November 2012.

[2] L. Cândido. Projeto de um UAV Solar de grande autonomia. Master's thesis, Universidade da Beira Interior, October 2014.

[3] T. Ferreira. Hybrid Propulsion System of a Long Endurance Electric UAV. Master's thesis, Instituto Superior Técnico, November 2014.

[4] D. Figueiredo. Autopilot and Ground Control Station for UAV. Master's thesis, Instituto Superior Técnico, November 2014.

[5] A. C. Marta. Long Endurance Electric UAV. Technical report, Instituto Superior Técnico, 2013.

[6] P. Miller. Remote Person View (RPV) for a Long Endurance Electric UAV. Master's thesis, Instituto Superior Técnico, May 2015.

[7] T. L. Saaty. *The Analytic Hierarchy Process: Planning, Priority Setting, Resource Allocation.* McGraw-Hil, 1980.

[8] N. Silva. Parametric Design, Aerodynamic Analysis and Parametric Optimization of a Solar UAV. Master's thesis, Instituto Superior Técnico, June 2014.

[9] H. Vidales. Design, Construction and Test of the Propulsion System of a Solar UAV. Master's thesis, Instituto Superior Técnico, March 2013.